Journal of
Nanoscience and Nanotechnology
Vol. 12, 7139–7147, 2012

Investigating Chiral Recognizability of Diastereomeric Crystallization of Mandelic Acid and L-Phenylalanine

Jong Min Kim[1], Sang Mok Chang[1], In Ho Kim[2], Xuan-Hung Pham[3], and Woo-Sik Kim[3,*]

[1] *Department of Chemical Engineering, Dong-A University, 604714, Korea*
[2] *Department of Chemical Engineering, Chungnam National University, 305764, Korea*
[3] *Department of Chemical Engineering, Kyung Hee University, 446701, Korea*

The present study investigated the mechanism of the chiral recognition of the resolving agent (L-phenylalanine) to the chiral isomers (D/L-mandelic acid). According the NMR analysis, the distinctive chemical shifts of between two diastereomer crystals (L-mandelic acid-L-phenlyalanine and D-mandelic acid-L-phenylalanine) were observed even though there was no difference of the chemicals shift of the two diastereomer solutions. This result indicated that the chiral recognition of the resolving agent mainly occurred during the crystallization of the diastereomers in the solution. Then, the chiral recognition of the diastereomers was confirmed by using thermal analysis and AFM. The diastereomer crystal of L-mandelic acid-L-phenylalanine was much more thermally stable due to the higher lattice energy than the diastereomer crystals of D-mamdelic acid-L-phenylalanine. Also, the adhesive force measured with AFM exhibited a stronger molecular interaction between L-mandelic acid and 4-amino-L-phenylalanine than between D-mandelic acid and 4-amino-L-phenylalanine. Plus, the AFM results implied that the hydroxyl group abundance on the mandelic acid surface was a possible explanation for the different chiral selectivity of the L-phenylalanine.

Keywords: Chiral Recognition, Crystallizing Separation, Chemical Force Microscopy, Nano Crystal, AFM Analysis, Affinity Force Measurement.

RESEARCH ARTICLE

1. INTRODUCTION

Chiral discrimination between enantiomers is currently one of the most important fields in supramolecular chemistry and analytical chemistry, especially for the pharmaceutical industry and clinical analysis. In addition, it is also related to the recognition fundamentals of biological systems, such as genes, proteins, enzyme-substrates, and antigen-antibodies. In the process of chiral discrimination, the functional groups in the molecular receptor preferentially interact with one of the enantiomers in the chiral molecule based on a noncovalent interaction, such as hydrogen bonding, electrostatic interaction, or hydrophobic interaction.[1] In many cases, while one enantiomer exhibits desirable physiological, pharmacological, pharmacodynamic, and pharmacokinetic properties, the other enantiomer can display toxicity towards living organisms and a different activity in chemical or biotechnological processes. Therefore, replacing the racemic form with a single-enantiomeric form in the drug market has further promoted the development of chiral recognition methods between two enantiomers.[2] As a result, various methods[3–10] have been found for determining the enantiomeric component of chiral compounds, as well as separating enantiomers from the racemate, such as NMR and DSC.

In the particular case of chiral molecules, the possible separation or enrichment of enantiomers through crystallization is of great academic and commercial interest, as crystallization is one of the most economical ways to obtain a high enantiomeric excess.[11] However, the use of crystallization in this context is limited by the observed behavior of chiral molecules isolated from racemic solutions. There are three possible outcomes during the crystallization of a racemic solution: (i) a racemic compound is formed in which each crystal contains a 1:1 mixture of enantiomers, (ii) a conglomerate appears that is a physical mixture of homochiral crystals, or (iii) a solid solution is formed consisting of heterochiral crystals. According to available data,[11,12] the formation of a racemic compound is the most common outcome. For this reason, the resolution of enantiomers is normally carried out through

*Author to whom correspondence should be addressed.

the use of chiral acids or bases to form diastereomeric salts. Unlike the enantiomers from which they are formed, diastereomers have different physical properties, including crystal formation, solubility, a melting point, and pharmacological activities[13] and thus can be easily separated from each other by crystallization. Hence, optical resolution via diastereomeric salt formation is the most practical method for obtaining pure enantiomers from a racemate on both a laboratory and industrial scale.[12, 14]

Even though diastereomeric crystallization was discovered by Pasteur nearly 160 years ago,[15] selecting the appropriate resolving agent still remains a significant challenge. Thus, to utilize diastereomeric crystallization for chiral separation, several recent studies have attempted to clarify the important physical properties of diastereomeric salts through the use of phase diagrams for solid–liquid equilibriums[16, 17] and estimating the molecular structure of less- and more-soluble diastereomeric salts.[18, 19]

Yet, despite such progress in chiral diasteromeric crystallization, the chiral recognition mechanism between enantiomers and the resolving agent has not been carefully examined, as there is no direct technique for measuring the interaction force between two enantiomers and the resolving agent. Several reports also showed the possibility of a chiral selective crystallization process from a racemic mandelic acid solution when applying L-phenylalanine (L-Phe) as the resolving agent. The different intermolecular structures were revealed by the crystal structure of the D-MA-L-Phe and L-MA-L-Phe salts.[20] The X-ray diffraction pattern for both the crystals was measured to reveal the role of the resolving agent by the function of the molecular ratio.[21] Both the papers indicated clearly the structural difference between the two diasteromeric crystals, and revealed the difference in the hydrogen bond made an important role for the diasteromeric crystal formation. On the other hand, Ichikawa et al. show a different kind of the binding force can be also related to the diasteromeric salt formation such as CH-π interaction and π–π interaction using a different kind of diasteromeric crystals.[22] In this way, various kinds of the interaction force can be involved in the chiral recognition techniques performed by the crystallization process, but the mechanism related to the selectiveness is unclear.[23]

Recently, the highly sensitive technique of atomic force microscopy (AFM) has been used to investigate mechanisms on a sub-molecular level, especially biological interactions. For example, the interaction forces of biotin-streptavidin,[24–26] complementary DNA strands,[27, 28] and antibody-antigen complexes[29, 31] have all been successfully explored. In principle, AFM records the force based on the deflection of the cantilever along the tip-surface distance.[32] Therefore, AFM could feasibly be applied to detect the interaction of a chiral enantiomer and a resolving-agent-modified tip on a sub nN level.[33]

Accordingly, this study demonstrates the potential for understanding the chiral recognition mechanism of a model system composed of chiral mandelic acid and a resolving agent (L-Phe) using AFM, NMR, and vibration spectroscopy. In addition, the physical properties of the two corresponding diastereomeric salts resulting from the resolving agent L-phenylalanine and two mandelic acid enantiomers are also examined using thermal analyses.

2. EXPERIMENTAL DETAILS

2.1. Chemicals

The enantiomers of mandelic acid and resolving agent L-phenylalanine (99% purity, TCI Company, Japan) were used as received. The 4-aminothiophenol (4-ATP), *p*-Toluenesulfonyl chloride (TSC), pyridine anhydrous, and 16-mercaptohexadecanoic acid (16-MHA), plus the materials for the IR, Raman, and NMR spectroscopy were all purchased from Sigma-Aldrich and used as received. Deionized water was used to prepare the two diastereomeric salts by cooling crystallization.

2.2. Diastereomeric Crystallization

The diastereomeric crystals of L-mandelic acid-L-phenylalanine and D-mandelic acid-L-phenylalaine were prepared by cooling crystallization in a double-jacketed Ruston reactor with a working volume of 50 mL. The individual enantiomers (D or L-form) of mandelic acid (50 g/L) were first dissolved in distilled water, followed by the equivalent molar addition of L-phenylalanine as the resolving agent. The solution was then heated to 80 °C to allow complete dissolution of the resolving agent. Thereafter, to induce diastereomeric crystallization, the solution was cooled to room temperature (25 °C) at a cooling rate of 10 °C/hr with gentle agitation at 200 rpm. After reaching room temperature, the solution was maintained at this temperature for 2 hrs. The crystals were then filtered out of the suspension using a 0.45 μm filter membrane and washed with ice water. The diastereomeric crystals were re-crystallized at least 3 times to eliminate any impurities. Finally, the retrieved crystals were dried in a vacuum oven at room temperature for 1 day and stored in an esiccators until analysis.

2.3. Modification of Tip and Sample for Chemical Force Microscopy

The probe tip of the AFM was coated with 4-amino-L-phenylalanine using the method suggested by Tsourkas.[34] For this purpose, two types of micro cantilever were selected for the tapping mode phase lag imaging (RTESPA, f = 320 kHz, k = 40 N/m, Veeco Inc., U.S.A.) and contact mode affinity force measurements (OMCL-TR400PB-1, k = 0.09 N/m, Olympus). The tapping mode probes were made of Si, and the probe tip coating with gold film (thickness = 10 nm) after an undercoating of

Ti film (thickness = 5 nm) was performed using a sputter technique. This process was necessary for further tip modification. The contact mode probe was originally purchased in an Au-coated form. The tip modification was performed following the cleaning procedure of the cantilever. The clean cantilevers were immersed in a 1 mM solution of 4-ATP in absolute ethanol for 24 hr to form a self-assembled monolayer. Next, the cantilevers were immersed in 0.2 M HCl solution to perform a diazotization coupling reaction with L-phenylalanine and washed carefully with absolute ethanol. More detailed procedure for the tip preparation was documented in our previous paper.[35] Meanwhile, mandelic acid was immobilized on the mica substrate using a two-step process. First, the mica was freshly cleaved to expose a molecularly flat surface, and then dipped into a 1 mM 1-octanethiol/ethanol solution for 1 hr to obtain a hydrophobic surface via a self assembly process. Second, a soft lithography technique was used to modify the surface with D- or L-MA.[36] For this purpose, a 2×2 μm^2 chrominium check pattern was used as the original mold,[37] and a stamp replica obtained using poly(dimethylsilozane). A 1 mM mandelic acid/hexane solution was used as the "ink." During the stamp process, a benzoic ring of mandelic acid was formed in response to the exposed carbon chain of self-assembled 1-octanethiol via a so-called hydrophobic interaction.[38] Based on trial and error, a concentration of 1 mM ink was eventually used, as the resulting pattern height was similar to the monolayer thickness. The finally obtained substrate was then carefully washed with flowing pure ethanol and dried with compressed N_2 gas.

2.4. Calibration of the Spring Constant

The calibration of the spring constant was performed by a well-known thermal fluctuation method.[39,40] For this purpose, a digital oscilloscope (WaveRunner 6050, Recroy) and an AFM instruments (SPI 4000, SII Nano) were used. In the calibration, the differential signal of the optical lever was monitored using the FFT function of the oscilloscope (f = 32 kHz). Next, to obtain the cantilever replacement data by the thermal fluctuation, the RMS differential level was firstly obtained using RMS calculating function of the AFM. To convert the obtained RMS voltage to cantilever displacement data, the sensitivity of the optical lever (mV/nm) was calculated using the repulsive force area in a measured force curve. The mica substrate was used for this measurement, and this calculation was performed by an automatic function of the AFM software. In the result, the cantilever displacement was corresponded to 0.2 nm at 25 °C. These values can be used to calculate the spring constant using the equitation reported by Ohler.[40]

In this way, the spring constant was calculated as 0.065 [N/m]. The spring constant of a sub-10^{-2} [N/m] level was not changed for the cantilevers in the same shipping package. Thus, the spring constant was evaluated as 0.06 N/m.

2.5. AFM Analysis

The AFM analysis of the L- or D-MA-modified surface was performed based on two techniques, phase lag mapping and contact force measurement, using L-Phe-modified probe tips. To obtain clear comparative results, the force measurement or phase lag mapping was conducted using the same cantilever for the D- or L-MA sample and the 1-octanethiol-modified surface. A nanoscope IV (Veeco Inc., Santa Barbara, U.S.A.) was used to take the measurements under ambient conditions at 20 °C (45% RH), and the analysis of the measured data was performed using SPIP® software.

2.6. NMR Analysis

An Advance 600 FT-NMR spectrometer system (Brucker, Germany) was used to investigate the chiral recognizability of the distereomeric crystals of mandelic acid-L-phenylalanine. The ^{1}H-NMR and ^{13}C-NMR were recorded in a solid state. The chemical shifts were reported in parts per million (δ).

2.7. FT-IR Spectroscopy

A sample of the diastereomeric crystals was carefully ground and passed through a 200 μm sieve. The KBr powder (200 mg) was then dried in a heating oven at 110 °C overnight, and mixed well with the sample powder (2 mg) in mortar. Next, the powder mixture was pelletized using a 12 kDa press for one minute and the pellet then dried again in the oven at 60 °C for 12 hrs.

Using a 2000 FT-IR spectrometer (Perkin Elmer, U.S.A.), the pellet was scanned from 4000 to 400 cm^{-1}. The scanning was repeated 100 times, resulting in an average spectrum with a spectral resolution of 4 cm^{-1}.

2.8. FT-Raman Spectroscopy

The FT-Raman spectra were measured using a RFS 100/s FT-Raman spectrometer (Brucker, Germany) equipped with a diode pumped Nd:YAG laser (200 nm) as the excitation source. For each spectrum, 100 scans were performed at a resolution of 4 cm^{-1} over a range of 0∼4000 cm^{-1}.

2.9. Thermal Analysis

The melting point and enthalpy of the diastereomeric crystals were measured using a DSC Q100 Photo-calorimeter (TA instruments, U.S.A.). Samples of the diastereomeric crystals sealed air-tightly in aluminum pans were thermally scanned from 300 to 573 K with a heating rate

of 5 K/min under a nitrogen atmosphere. Meanwhile, the temperature range of the thermal decomposition was determined based on a thermo-gravimetric analysis performed using a TGA Q5000 IR system (TA Instruments, U.S.A). The sample chamber was purged with N_2 gas at a flow rate of 50 cm^3 min^{-1}.

3. RESULTS AND DISCUSSION

3.1. Chiral Recognition in Diastereomeric Salts Using NMR Spectroscopy

The intermolecular interaction of L-Phe with MA in the liquid phase NMR analysis was so weak and non-selective that no chiral recognizability of the diastereomeric salts was detected. Thus, the chiral recognition of the diastereometic salts was investigated in a solid state. Here, the two corresponding solid diastereomeric salts were prepared by co-crystallizing enantiomeric D- or L-MA with L-Phe, as explained in the Experiment section above. Thereafter, solid state NMR, FT-IR, and FT-Raman analyses of the crystals were performed to compare the differences of the inter-molecular structures. In Figure 1, the magnetic absorption overlap of the protons in the solid state complicated the discrimination of the two diastereomeric salts. However, Figure 1(a) shows a dramatic difference between the COOH proton in the L-MA-L-Phe (14 ppm) and the COOH proton in the D-MA-L-Phe (12 ppm), indicating that the chiral recognition was due to the COOH group.[41] In our recent papers, we reported the polarity change of the COOH group influence the diasteromeric crystal formation because the number of the hydrogen bond could be differently produced by the polarity.[21,35] In addition, Figure 1(b) shows the different resolution of the COOH group at 175 ppm which implies the different functionality of the COOH group between the two diasteromeric salts.

The use of the solid-state ^{13}C-cross-polarization-magnic-angle-spinning (^{13}C CP/MAS) technique at room temperature with a spinning rate of 12 kHz also allowed the two diastereomeric salts to be more clearly discriminated (Fig. 1(b)).[42] Thus, for the diastereomeric salts, the carbon that appeared at $\delta = 36.5$ ppm (D-MA-L-Phe) and $\delta = 38.2$ ppm (L-MA-L-Phe) corresponded to the methylene carbon (CH_2) in the L-Phe, while the carbon singlet peak at $\delta = 58$ ppm corresponded to the methine carbon (CH) in the L-Phe. Meanwhile, the methine carbon in the MA appeared at $\delta = 72.2$ ppm for the D-MA-L-Phe and $\delta = 74.7$ ppm for the L-MA-L-Phe. The difference between the molecular structures of the two diastereomeric salts was also expressed by the carbon in COOH, which appeared at $\delta = 174.2$ ppm for the D-MA-L-Phe and $\delta = 176.3$ ppm for the L-MA-L-Phe. Since the carbon in methine is adjacent to the ammonium cation, as well as the carboxyl group, these carbons must be significantly influenced by the chiral moiety and shifted, as demonstrated by the results.

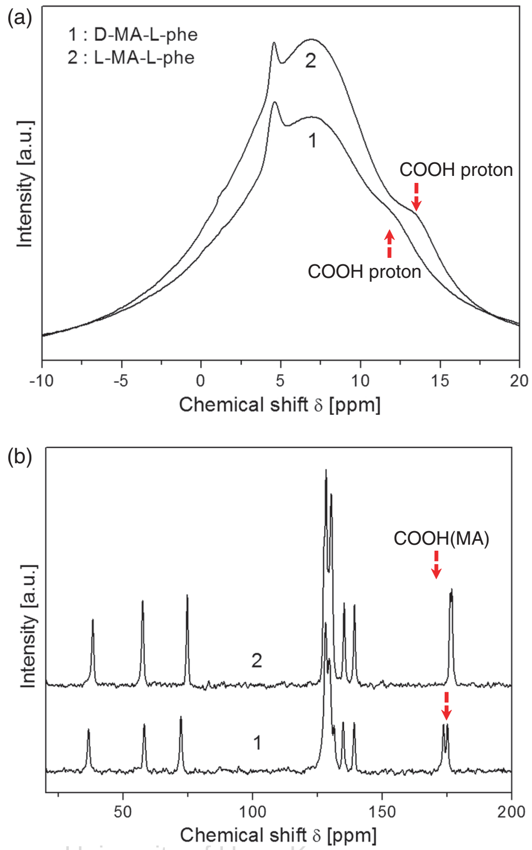

Fig. 1. Solid state NMR spectroscopy of two diastereomeric salts. (a) ^1H-NMR, (b) ^{13}C-NMR. 1. D-mandelic-L-phenylalanine, 2. L-mandelic-L-phenylalanine.

In summary, the NMR results indicated that the chiral discrimination of MA by L-phenylalanine occurred at COOH, plus both the carbon and proton peaks of the D-MA-L-Phe diastereomer were lower than those of the L-MA-L-Phe diastereomer. Furthermore, the solid state NMR revealed that the phenyl ring of L-Phe had no effect on the chiral recognition of MA by L-Phe, as the phenyl carbon in the two diastereomers displayed a similar multiplet at $\delta = 126$ to $\delta = 140$ ppm.

3.2. Chiral Recognition Analysis in Diastereomeric Salts Using Vibration Spectroscopy

FT-IR and FT-Raman spectroscopy were also used to discriminate between the two diastereomeric salts of D-MA-L-Phe and L-MA-L-Phe. In the 1500–1800 cm^{-1} region, the IR (Fig. 2(a)) and Raman spectra (Fig. 2(b)) for the two diastereomers contained three vibrational bands (Fig. 2). The most prominent peak occurring at 1606 cm^{-1} was assigned as the phenyl CC quadrant stretching mode.[43] Meanwhile, the lowest energy band occurring at 1700 cm^{-1} corresponded to the COO-group,[44] and the shoulder at 1645 cm^{-1} was likely due to a NH^{2+} deformation mode.

In the 2000–3500 cm^{-1} region of the spectra (Fig. 3), the two diastereomers contained a cluster of peaks between

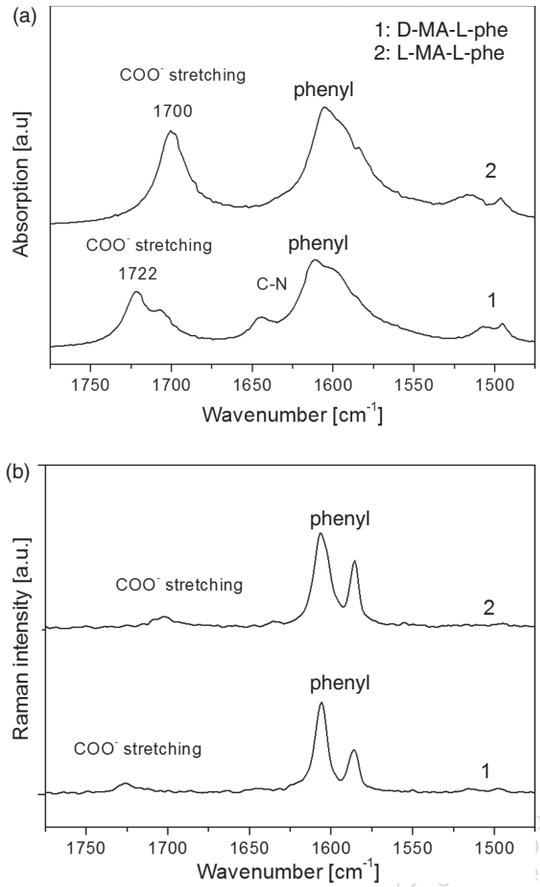

Fig. 2. Vibrational spectroscopy of two diastereomeric salts within wavenumber range of 1500–1800 cm^{-1}. (a) IR spectroscopy, (b) Raman spectroscopy. 1. D-mandelic-L-phenylalanine, 2. L-mandelic-L-phenylalanine.

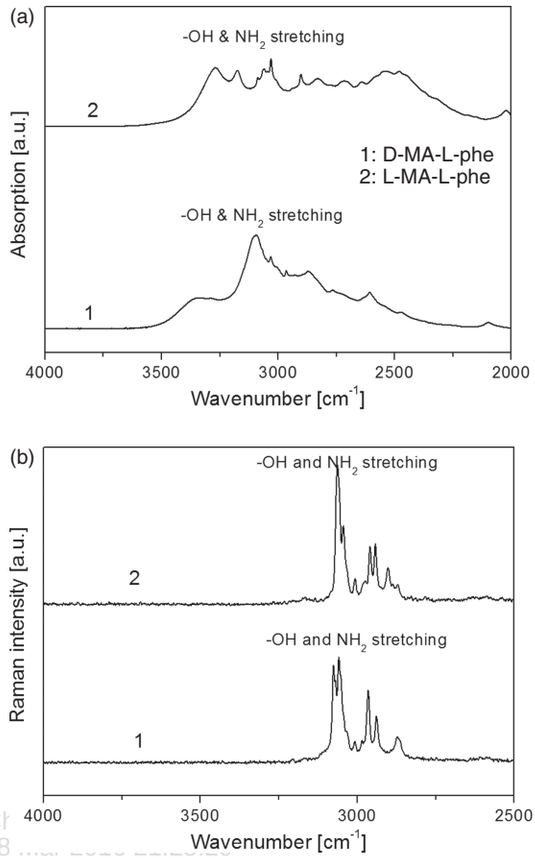

Fig. 3. Vibrational spectroscopy of two diastereomeric salts within wavenumber range of 2000–4000 cm^{-1}. (a) IR spectroscopy, (b) Raman spectroscopy. 1. D-mandelic-L-phenylalanine, 2. L-mandelic-L-phenylalanine.

2800 and 3025 cm^{-1}, corresponding to the aliphatic CH_2 and CH from MA and L-Phe.[44] Plus, the shoulder peak at 3050–3100 cm^{-1} corresponded to thes overlapping peaks of NH_2 and OH.

Even though the two diastereomers had the same chemical structure, as they were both made of MA and L-Phe, their IR and Raman spectra were significantly different in the vibrational mode. In the case of the IR spectra for the L-MA-L-Phe diastereomer, the COO^- asymmetric stretching peak occurred at 1700 cm^{-1}, while the NH_2 deformation nearly disappeared due to an overlap with the phenyl CC quadrant stretching mode. The Raman spectra confirmed the same results.

In the case of the D-MA-L-Phe diastereomer, the COO^- asymmetric stretching peak occurred at 1722 cm^{-1} and the NH_2 deformation at 1645 cm^{-1}. According to literature, COO^- asymmetric stretching vibrates at 1750 cm^{-1} and its shift is dependent on the hydrogen bonding force. Thus, the L-MA-L-Phe had a stronger hydrogen bonding force, as its wavenumber shift compared to the standard COO^- stretching wavenumber was about 30 cm^{-1}, which was higher than that for the D-MA-L-Phe at 18 cm^{-1}. Moreover, OH and NH_2 asymmetric stretching was also revealed in the region of 3050 to 3100 cm^{-1}, as mentioned above. In the D-MA-L-Phe, the OH and NH_2 stretching was at 3065 cm^{-1}, while in the L-MA-L-Phe, it remained at 3050 cm^{-1}.

Therefore, the IR and Raman spectral patterns revealed that both L-MA and D-MA formed unique diastereomers with L-Phe, and the difference in the vibrational spectral mode of the two diastereomers suggested that COOH, NH_2, and OH (only contained in MA) played the important roles in the chiral discrimination of MA by L-Phe due to a different hydrogen bonding pattern.

3.3. Direct Measurement of Affinity Force by Chemical Force Microscopy

To show the affinity difference between the modified L- or D-MA surface and L-Phe, two techniques of chemical force microscopy, direct contact force measurement and phase lag mapping, were used with applying L-Phe-modified probe tips. Unfortunately, measuring the single

molecular order direct affinity force between modified and sample materials is normally difficult, especially when the molecular size is small. Thus, the present approach was based on a statistical method after obtaining numerous affinity force data (affinity image). As explained in the experimental section, the two functional groups (COOH and OH) of D- or L-MA were possibly exposed on the sample surface by the sample fabrication procedure. Thus, the affinity difference between the two functional groups of D- or L-MA and L-Phe (functional group COOH and NH_2) were obtained using L-Phe-modified probe tips.

Figure 4 shows the typical force curve data (Figs. 4(a, b)) and statistical data (Figs. 4(c, d)) for D-MA and L-MA when using a L-Phe modified cantilever. Both force curves were obtained using the same microcantilever modified with L-Phe. In the case of D-MA, the short range attractive force was about 200 pN and the long range adhesive force was about 8.5 nN. Meanwhile, for the L-MA surface, the short range attractive force was about 920 pN and the long range adhesive force was about 16 nN. Thus, both the attractive and adhesive forces were high for L-MA. Figures 4(c) and (d) show a statistical result of the force curve measurement for D-MA (Fig. 4(c)) and L-MA (Fig. 4(d)). To obtain the result, a 500 force curve measurement was performed for each surface. In the result, the sub-nN order force was discarded for the simple graphic illustration. For example, the range of the force for 1 nN corresponds to 1 nN ∼1.99 nN. In fact, a number of the cantilevers were required for the measurement because of the tip and sample contamination. For example, 2 nN force range in Figure 4(c), 9 nN and 23 nN force range in Figure 4(d) were assumed to be obtained by the possible contamination. The statistical result confirms the adhesion force of the D-MA is small compared with that of the L-MA though the spectrum are scattered in a wide force area. For further confirmation of the result, we had performed another force measurement with unmodified hydrophilic bare Au coated tip. The hydrophilicity of the bare Au-tip was previously reported.[32] In the case of the D-MA surface, a large portion of the measured force was located at 2 nN, and the measured spectra width is small except 13 nN area. The 13 nN adhesive force seems to be obtained by the tip or sample damage. Thus, a mean adhesive force of 2 nN was measured. This intensity of the

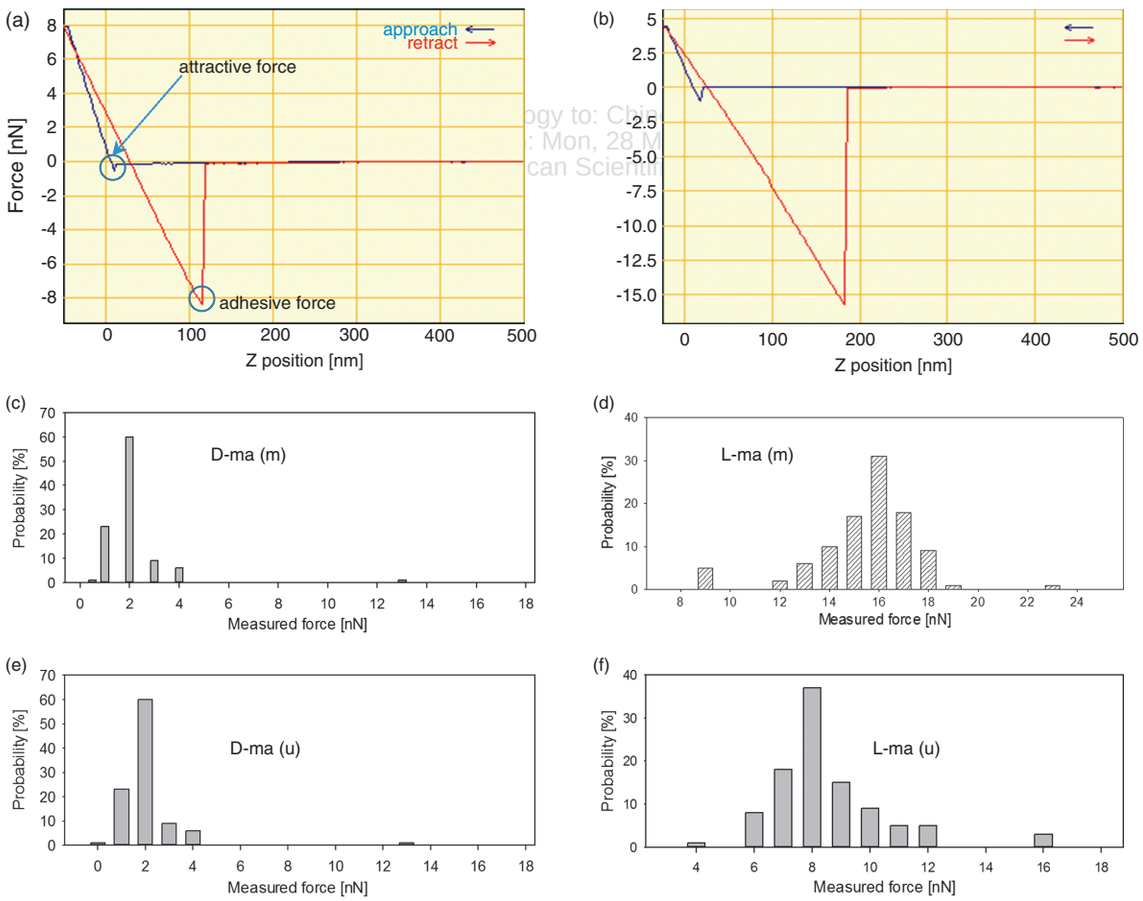

Fig. 4. Contact mode force mapping using L-Phe-modified probe tip for D-MA (a) and L-MA (b) surface. (c) and (d) show a statistical result for the 500 cycle force curve measurement for D-MA (c) and L-MA (d) surfaces with L-Phe modified tips. (e) and (f) shows a statistical result for the 500 cycle force curve measurement for D-MA (e) and L-MA (f) surfaces with bare Au coated tips.

RESEARCH ARTICLE

adhesive force was comparable with 8 nN for the L-MA surface. The comparison implied the L-MA surface had a strong adhesive force than the D-MA surface explainable by the different capillary force. Thus, different surface structure could be expected between the two surfaces. As the strong adhesive force made it difficult to obtain a clear surface topography, the affinity interaction was also measured using phase lag mapping imaging, which is a tapping mode technique that shows the phase difference between the driving oscillation of the piezoelectric oscillator and the oscillation of the cantilevers as they interact with the sample surface.[45] Normally, the phase lag reveals the different adhesion force, friction, and viscoelasticity. Thus, a strong adhesive force can produce a strong phase lag signal, meaning a strong binding interaction.

Figure 5 shows the phase lag mapping results when using a L-Phe modified tapping mode cantilever with 1-octanethiol (Figs. 5(a and b)), D-MA (Figs. 5(c and d)), and L-MA (Figs. 5(e and f)). As shown in Figures 5(a) and (b), 1-octanethiol was compactly assembled on the mica surface, where the evaluated RMS roughness was about 0.32 nm with a mean height of 1.2 nm, indicating the surface was successfully modified with 1-octanethiol. Plus, the phase lag intensity of the 1-octanethiol was normally within a range of 15°, meaning no interesting interaction force between the L-Phe-modified tip and the 1-octanethiol. (Note; the image contrast in Figures 5(b), (d), and (f) was arbitrarily controlled for a clear appearance). The bright area (relatively strong phase lag signal) in Figure 5(b) seems to be an unmodified area of the mica, as the carboxyl group of L-Phe has a slight interaction force with the unmodified hydrophilic mica surface, although the intensity is within 15°, as shown in the line profile analyses (Fig. 5(h)). For the D- or L-MA-modified surfaces in Figures 5(c) and (e), the grain size and mean height were increased with the addition of MA. In the line profile analyses of the topography images (Fig. 5(g)), the heights of the two surfaces were similar, while the horizontal distance of the grains meant that both surfaces were aggregated by the added molecules. The major difference between the two topography images was the particle boundary areas, indicated by arrows in Figure 5(e) and not observed in Figure 5(c). Observed over the entire topography image for L-MA, these particle boundary areas mean that no clear boundaries were obtained and thus can be treated as topography errors, as the probe tip was unable to reach the solid surface. In addition, the black boxed area in Figure 5(e) represents a topography profiling delay during the scan, indicating unsuccessful AFM feedback in this area, and thus can also be treated as a signal error. An explanation of these topography errors is provided by the phase lag images in Figures 5(d) and (f), both of which were successfully obtained based on just the tip separation time from the surface. As a result, the range of the phase lag intensity was also different in Figures 5(d) and (f).

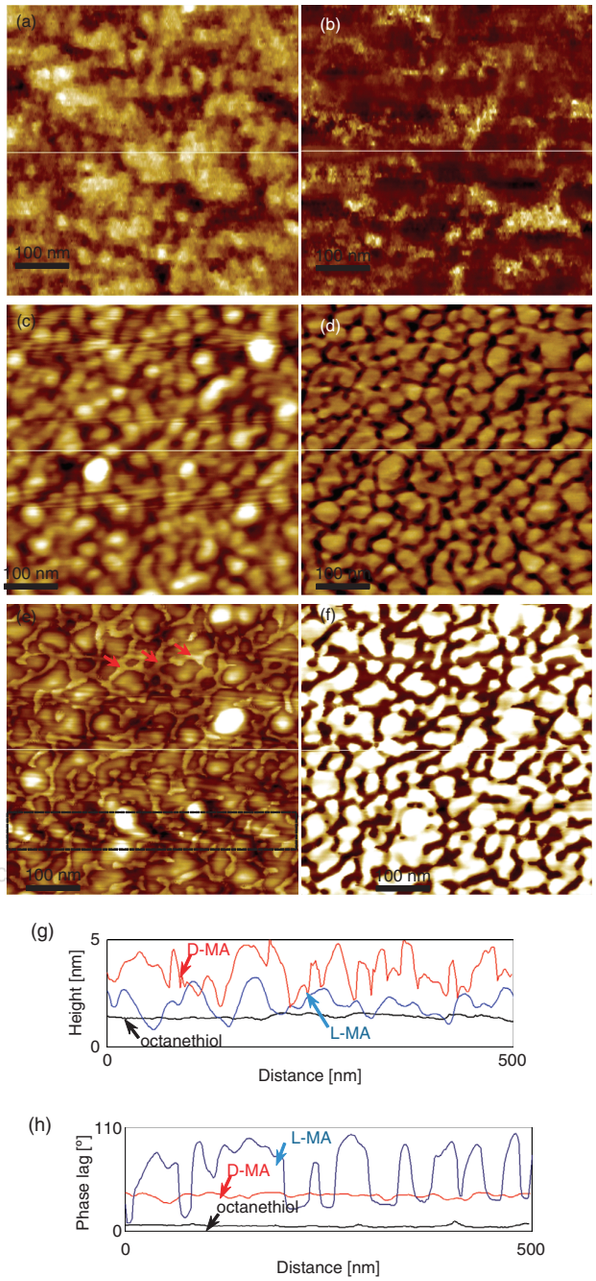

Fig. 5. Tapping mode phase lag mapping using L-Phe-modified probe tip. (a) and (b) show 1-octanethiol-modified surface, (c) and (d) show D-MA-modified surface, (e) and (f) show L-MA-modified surface for topographic image (a, c, and e) and corresponding phase lag images (b, d, and f). (g) and (h) show line profile analyses of topographic images and phase lag images, respectively.

In the case of D-MA, the range was within 40°, whereas for L-MA, the range was within 90°. Thus, the tip separation of D-MA was easily compared with that of L-MA, and revealed a stronger adhesive force between L-MA and the L-Phe modified probe tip than between D-Ma and the probe tip. Importantly, these phenomena occurred across all the image areas in Figures 5(d) and (f). Thus, it was

RESEARCH ARTICLE

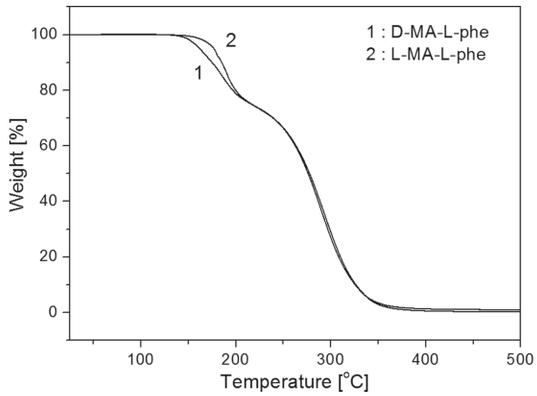

Fig. 6. TGA spectra of two diastereomeric salts. 1. D-mandelic-L-phenylalanine, 2. L-mandelic-L-phenylalanine.

concluded that the overall surface area of L-MA had a stronger affinity force towards L-Phe than the D-MA surface area. This strong affinity force then made it difficult to control the feedback, resulting in the topography errors for the L-MA image.

In summary, the different surface functionality of D- or L-MA was investigated using a CFM technique. The chemical affinity force measurement revealed that the adhesion force of L-MA was nearly two-fold higher than that of D-MA, and this was also confirmed by the phase lag mapping results. For the current measurement, the difference in the hydrogen bonding number or van der Walls force was a possible mechanism for the measured adhesive force difference. As L-Phe was used in both the measurements, the difference may have also come from the surface difference between D-MA and L-MA. Thus, a possible conclusion is that the exposed hydroxyl group on the aggregated MA surfaces was clearly different due to the different 3D structures of the enantiomers. For clearer conclusion of the result, further study on the property of the surface such as molecular aggregation structure and molecular strength is required especially for the 3-dimensional crystal growth mechanism.

3.4. Chiral Recognition of D/L-mandelic Acid by L-phenylalanine Based on Thermal Analysis

Several recent studies have already demonstrated the relationship between the crystal structure and the physicochemical properties of a pair of diastereomeric salts.[46, 47] As such, the difference in the solubility between a pair of diastereomeric salts has been associated with a difference in their respective melting points and enthalpies of fusion. Thus, the present study applied a thermal analysis to investigate the thermal stability of the two diastereomeric salts in relation to their crystal structural stability. As a result, thermal gravimetry (Fig. 6) and differential scanning calorimetry[35] confirmed that the L-MA-L-Phe with a melting point at 185.4 °C was more thermally stable and less soluble in a solution than the D-MA-L-Phe (159.5 °C). The heat fusion of the diastereomeric salts, representing the host-guest interaction, also agreed with the TGA data, as the enthalpy for the L-MA-L-Phe was 380 J/g, while the enthalpy for the D-MA-L-Phe was 321 J/g. The broad shoulder and small peaks were obtained after the melting for both the diasteromeric salts. These were related to the simultaneous decomposition of MA after melting. Thus, these were not obtained in the second heating cycle. Consequently, the analysis results indicated that the diastereomeric salt of L-MA-L-Phe with a higher thermal stability and lattice energy was certainly expected to be crystallized out from the solution, as consistent with the experimental results.

4. CONCLUSION

Based on differences in the molecular structure, chiral recognition was successfully achieved by comparing the physicochemical properties of two diastereomeric salts resulting from chiral enantiomers and a resolving agent. According to the thermal analysis, it was proved that the diastereomer of L-mandelic acid-L-phenylalanine was more thermally stable due to the higher lattice energy, indicating the preferential formation of its diastereomer crystals when compared to the diastereomer of D-mandelic acid-L-phenylalanine. Moreover, it was found that the adhesive force between L-mandelic acid and L-phenylalanine (16 nN), representing the hydrogen bonding and van der Waals force etc., was stronger than that between D-mandelic acid and L-phenylalanine (7 nN) based on measuring the contact AFM using a tip modified with the resolving agent. The possible mechanism of this different affinity interaction may help in the further development of chiral-selective crystallization.

Acknowledgment: This study was financially supported by NRF Research Funding (Korea, 2010-0017993).

References and Notes

1. E. Kocabas, M. Durmaz, S. Alpaydin, A. Sirit, and M. Yilmaz, *Chirality* 20, 26 **(2008)**.
2. E. L. Izake, *J. Pharm. Sci.* 96, 1659 **(2007)**.
3. R. Liu, Z. Chen, F. Zhao, X. Chang, Y. Zu, and X. Guo, *J. Nanosci. Nanotechnol.* 11, 7587 **(2011)**.
4. J. M. Kim, S.-M. Chang, F. Li, H. Guo, and W.-S. Kim, *J. Nanosci. Nanotechnol.* 11, 7676 **(2011)**.
5. E. Chen, B. Guo, B. Zhang, L.-H. Gan, and J. R. Gong, *J. Nanosci. Nanotechnol.* 11, 7682 **(2011)**.
6. Y. Chen, Y. Chen, Y. Li, M. Zhang, X. Liu, B. Li, and Y. Yang, *J. Nanosci. Nanotechnol.* 11, 4073 **(2011)**.
7. J. Kiang-ia, H. Hailong, Y. Bin, Y. Jantippana, P. Pantu, J. Limtrakul, N. Chattham, S. Zexing, and Y. Ting, *J. Nanosci. Nanotechnol.* 10, 7208 **(2010)**.
8. J. Yan, B. Li, S. Wang, Y. Chen, Y. Li, G. Zhu, and Y. Yang, *J. Nanosci. Nanotechnol.* 10, 6732 **(2010)**.

9. P. Nikolaev, W. Holmes, E. Sosa, P. Boul, S. Arepalli, and L. Yowell, *J. Nanosci. Nanotechnol.* 10, 3780 **(2010)**.
10. S. Roy, S. Basak, and A. Kr. Dasgupta, *J. Nanosci. Nanotechnol.* 10, 819 **(2010)**.
11. J. Jacques, A. Collet, and S. H. Willen, Enantiomers, Racemates and Resolution, Wiley and Sons, New York **(1994)**.
12. C. P. Brock, W. B. Schweizer, and J. D. Dunitz, *J. Am. Chem. Soc.* 113, 9811 **(1991)**.
13. N. Vaidya, *Spec. Chem. Mag.* 26, 40 **(2006)**.
14. P. Newman, Optical Resolution Procedures for Chemical Compounds, edited by P. Newman, Optical Resolution Information Center, Manhattan College, New York **(1984)**, Vol. 2.
15. L. Pasteur and C. R. Hebd, *Seances Acad. Sci.* 162, 277 **(1854)**.
16. A. Maria, N.-B. Elisabeth, S. Kalman, and A. Gyula, *J. Chem. Soc. Perkin Trans.* 2, 2011 **(1992)**.
17. E. Ebbers, J. Gerry, A. Ariaans, B. Zwanenburg, and A. Bruggink, *Tetrahedr A* 9, 2745 **(1998)**.
18. K. K. Éva, G. M. Keserü, Z. Böcskei, L. Szilágyi, K. Simon, B. Bertók, and E. Fogassy, *J. Chem. Soc. Perkin Trans.* 2, 149 **(2000)**.
19. K. Kinbara, Y.Kobayashi, and K. Saigo, *J. Chem. Soc. Perkin Trans.* 2, 1767 **(1998)**.
20. K. Okamura, K. Aoe, H. Hiramatsu, N. Nishimura, T. Sato, and K. Hashimoto, *Anal. Sci.* 13, 315 **(1997)**.
21. X.-H. Pham, J. M. Kim, S.-M. Chang, and W.-S. Kim, *J. Mol. Cat. B* 60, 87 **(2009)**.
22. A. Ichikawa, H. Ono, T. Echigo, and Y. Mikata, *Cryst. Eng. Comm.* 13, 4536 **(2011)**.
23. E. L. Florin, V. T. Moy, and H. E. Gaub, *Science* 264, 415 **(1994)**.
24. G. U. Lee, D. A. Kidwell, and R. J. Colton, *Langmuir* 10, 354 **(1994)**.
25. S. S. Wong, E. Joselevich, A. T. Woolley, C. L. Cheung, and C. M. Lieber, *Nature* 394, 52 **(1998)**.
26. L. H. Pope, M. C. Davies, C. A. Laughton, C. J. Roberts, S. J. Tendler, and P. M. Williams, *Eur. Biophys. J.* 30, 53 **(2001)**.
27. T. Strunz, K. Oroszlan, R. Schäfer, and H. J. Güntherodt, *PNAS* 96, 11277 **(1999)**.
28. S. Allen, X. Chen, J. Davies, M. C. Davies, A. C. Dawkes, J. C. Edwards, C. J. Roberts, J. Sefton, S. J. Tendler, and P. M. Williams, *Biochemistry* 36, 7457 **(1997)**.
29. U. Dammer, M. Hegner, D. Anselmetti, P. Wagner, M. Dreier, W. Huber, and H. J. Guentherodt, *Biophys. J.* 70, 2437 **(1996)**.
30. P. Hinterdorfer, W. Baumgartner, H. J. Gruber, K. Schilcher, and H. Schindler, *PNAS* 93, 3477 **(1996)**.
31. G. Zavala, *Colloid Polym. Sci.* 286, 85 **(2008)**.
32. J. M. Kim and H. Muramatsu, *Nano Lett.* 5, 309 **(2005)**.
33. J. M. Kim, H. S. Jung, J. W. Park, H. Y. Lee, and T. Kawai, *Anal. Chim. Acta.* 525, 151 **(2004)**.
34. S. Zhang, J. J. Ding, Y. Liu, J. Kong, and O. Hofstetter, *Anal. Chem.* 78, 7592 **(2006)**.
35. H.-S. Guo, J. M. Kim, X.-H. Pham, S.-M. Chang, and W.-S. Kim, *Cryst. Growth. Des.* 11, 53 **(2011)**.
36. T. Pfohl, J. H. Kim, M. Yasa, H. P. Miller, G. C. L. Wong, F. Bringezu, Z. Wen, L. Wilson, M. W. Kim, Y. Li, and C. R. Safinya, *Langmuir* 17, 5343 **(2001)**.
37. J. M. Kim, T. Ohtani, S. Sugiyama, T. Hirose, and H. Muramatsu, *Anal. Chem.* 73, 5984 **(2001)**.
38. S. Matsunaga, R. Yokomori, D. Ino, T. Yamada, M. Kawai, and T. Kobayashi, *Electrochem. Commu.* 9, 645 **(2007)**.
39. J. L. Hutter and J. Bechhoefer, *Rev. Sci. Instrum.* 64, 1868 **(1993)**.
40. B. Ohler, *Rev. Sci. Instrum.* 78, 063701 **(2007)**.
41. C. A. Lepre, J. M. Moore, and J. W. Peng, *Chem. Rev.* 104, 3641 **(2004)**.
42. D. Tapu, D. A. Dixon, and C. Roe, *Chem. Rev.* 109, 3385 **(2009)**.
43. N. B. Colthup, L. H. Daly, and S. E. Wiberly, Introduction to Infrared and Raman Spectroscopy Academic Press, London **(1990)**.
44. R. B. Silverstein, F. X. Webster, and D. J. Kiemle, Spectrometric Identification of Organic Compounds, John Wiley & Son, California **(2005)**.
45. J. M. Kim, S.-M. Chang, H. Muramatsu, and I. Karube, *Korean J. Chem. Eng.* 28, 987 **(2011)**.
46. R. Sakurai, O. Itoh, A. Uchida, T. Hattori, S. Miyano, and M. Yamaura, *Tetrahedron* 60, 10533 **(2004)**.
47. R. J. Prankerd and M. Z. Elsabee, *Thermochim. Acta.* 248, 147 **(1995)**.

Received: 31 March 2012. Accepted: 2 May 2012.